JMES The International Journal of
Mechanical Engineering and Sciences
https://journal.its.ac.id/index.php/jmes/index
e-ISSN 2580-7471

Influence of Confined Channel on the Self-Starting Capability of Twin Counter-Rotating Savonius Hydrokinetic Turbines in Tandem Arrangement

Hildan Fahrizal Nur Faurizki[1,2*], Tri Yogi Yuwono[2], Savitri Ramadhani[1,2], Vena Rizky Pusparani[3], Anisah Nurul Izzah[4], Chezta Ahmad Muzakky[3], Muhammad Fiky Izzulhaq[3]

[1]Department of Mechanical Engineering, Politeknik Negeri Semarang, Tembalang, Semarang 50275, Indonesia
[2]Department of Mechanical Engineering, ITS, Sukolilo, Surabaya 60111, Indonesia
[3]Politeknik Perkapalan Negeri Surabaya, Sukolilo, Surabaya 60111, Indonesia
[4]Department of Mechanical Engineering, Universitas Pembangunan Nasional Veteran Jawa Timur, Surabaya 60294, Indonesia

Received: 25 Juni 2026, Revised: 20 July 2026, Accepted: 29 July 2026

Abstract

This research aims to improve the Savonius turbine's self-starting capability by increasing the static torque coefficient using several methods. In this research, a channel and an additional turbine were applied to optimize the energy harvested from hydropower using a numerical approach. The configurations were of six blockage levels (0.61, 0.45, 0.3, 0.22, 0.1, and 0.05) and two distances (shorter at $2.667D$ and longer at $60D$) with a Reynolds number of 37000. The optimum self-starting capability was achieved at a blockage ratio of 0.61 for the $2.667D$ configuration. A 113.75% improvement at an azimuth angle of $60°$ for the upstream turbine, and a 229.21% improvement took place at an azimuth angle of $90°$ for the downstream turbine. At $60D$, almost the entire self-starting capability at several blockage levels experienced an increase. The optimum improvement at an azimuth angle of $60°$ and a blockage ratio of 0.61, with 113.08% and 110.22% for the upstream and downstream turbines, respectively. These key findings indicated that the installation of a Savonius turbine within a channel generates a higher self-starting capability by increasing the static torque coefficient, allowing the turbine to rotate more easily, and leading to greater dynamic torque and power.

Keywords: Savonius Hydrokinetic Turbine, Blockage, Self-starting, CFD, Renewable Energy

1. Introduction

Energy is essential for the human population; therefore, its demand is ever-increasing. As the primary energy source of today, fossil fuels are classified as non-renewable energy that needs to be reduced; thus, the renewable energy transition has become a worldwide priority. Renewable energy provided by the environment is abundant and sustainable, with hydro as one of the resources. Power is harvested from the water using a vertical- or horizontal-axis hydrokinetic turbine. As mentioned by [1], among 76 studies related to the turbines, the vertical-axis turbine has 33% research, development, and demonstration efforts, among others. One of the applications of vertical-axis turbines to harvest hydropower is the Savonius turbine, which produces torque and operates due to the drag difference that occurs on the advancing and returning blades. Although the Savonius turbine construction is simple, its performance is low. This has piqued many researchers' interest in increasing its performance. Moreover, since [2] stated that there are limited studies of Savonius research, particularly those related to the water channel and multi-turbine installation, this study aims to fill that gap.

Some studies about improving conventional Savonius turbine performance have been developed, many of which implemented several methods. [3–7] Investigated the influence of circular, I, and D cylinders as passive flow control on the Savonius turbine's performance with a range of 18.04%-41.18% enhancement in several optimum configurations. However, there is no further investigation of wall channel effects in the related studies. [8] explored the effect of a circular cylinder on the self-starting capability of a Savonius turbine, and it was found that the position of a cylinder plays a key role in controlling the self-starting capability. Research involving a deflector as a flow guide to one of the Savonius blades was conducted by [9–17]. Despite its purpose to direct the fluid flow, the existence of the deflector also has an objective as a disturbance toward the returning blade, which reduces the pressure drag on the returning blade. The drag reduction in the returning blade and flow guide toward the advanc-

*Corresponding author. Email: hildan.fahrizal@polines.ac.id, phone: +6281232266135

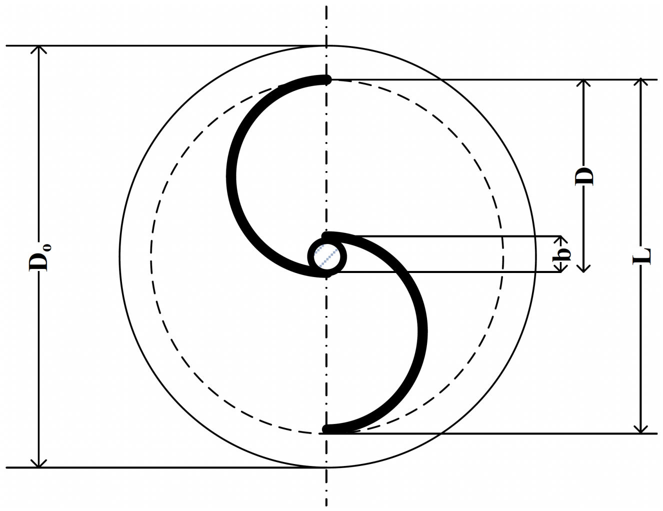

Figure 1. 2D geometry of Savonius hydrokinetic turbine.

ing blade is expected to improve the turbine performance by concentrating the momentum on the advancing blade. Nevertheless, the investigation in related research does not involve blockage levels in a water channel by varying the wall channel distance. Furthermore, several multi-Savonius turbine installations in various configurations in order to optimize the harvested power were investigated by [18–26]. According to the experiment of twin counter-rotating Savonius hydrokinetic turbines in a tandem arrangement with a certain horizontal distance (H_c) and rotor diameter (D_R) by [18]. It was known that counterclockwise (CCW) turbine performance was enhanced when $H_c/D_R < 0.73$. In contrast, clockwise (CW) turbine performance was enhanced at $H_c/D_R > 0.73$. But the conducted Savonius turbine was installed as a cross-flow with the advancing blade near the test section floor; furthermore, a wall channel was only at the test section floor. Research about twin-Savonius turbines in tandem arrangement was also carried out by [19–22], with the result that requires far enough distance for the downstream to be separated from the effect of the upstream turbine. By varying the distance of the two Savonius turbines, it was concluded that the downstream turbine's performance rises as the distance increased. [22] studied twin counter-rotating hydrokinetic Savonius turbines installed in a channel corresponding to a 0.22 blockage level using a numerical approach. The Savonius turbines were installed in a tandem array, with the distance between the upstream and downstream turbines (T) set at $2.667D$, $3.667D$, $13.667D$, $35D$, $40D$, $45D$, $50D$, $55D$, and $60D$; D is a blade diameter. At a distance of $2.667D$, the upstream wake shedding was extremely affecting the downstream turbine, leading to a decline in operational range or TSR. Conversely, at a distance of $60D$, the wake from the upstream turbine dissipates, allowing the downstream turbine to operate independently, similar to a single turbine. However, the study does not involve a blockage variation; hence, it motivates the current study to observe the influence of blockage levels on the twin Savonius hydrokinetic turbines.

Installation in a confined channel and its influence on the Savonius turbine were traced by [27–34]. [35] considered a blockage due to the additional narrowing effect in channel installation. [27], [29–34] mentioned that the increase in blockage or confinement level directs the Savonius turbine to perform with massive performance improvement, with a range of 33.33%-128%. This massive improvement occurs due to the higher pressure drag experienced by the Savonius turbine, which influences the production of dynamic torque and generated power. Furthermore, the operational range or Tip Speed Ratio (TSR) is also exceeded due to the energy conversion that comes not only from the kinetic energy, but also from the greater pressure drag in line with the installation in a water channel corresponding to the presence of the blockage. The phenomenon showed strong agreement with research conducted by [36], [37]. Further, [28] developed a velocity correction method to correct hydrokinetic turbine performance and produced a correction method that showed a similar result for the confined case when compared to the unconfined cases. The correction method is required to calculate the actual performance of the turbine.

Several previous studies have researched single turbines in channels or twin turbines in unconfined flows, while none investigated the combined influence of channel blockage and turbine proximity on the self-starting capability of twin counter-rotating Savonius hydrokinetic turbines. Hence, the novelty of this numerical study is twin Savonius hydrokinetic turbines installed in a confined channel with varying blockage levels and distances. This investigation is beneficial for the application of hydrokinetic turbines in rivers or other water channels, since the environment provides low-velocity conditions. The enhancement of the self-starting capability in the application of Savonius hydrokinetic turbines in low-velocity conditions is mandatory for higher production of static torque. In order to obtain comprehensive knowledge, six levels of blockage were used in this study along with two levels of horizontal distance between twin counter-rotating Savonius turbines.

2. Numerical Method

2.1. Governing Equations

In numerical studies, the governing equations involved in recent years are mass conservation, generally known as the continuity equation, and the Navier-Stokes equations. ANSYS Fluent 2023 R2 was used to solve the governing equations. Corresponding equations were solved in this numerical study with assumptions, i.e., steady, incompressible, 2-dimensional (XY-direction) flow, and negligible body force. The following Equations, 1 and 2, respectively, represent the continuity and Navier-Stokes equations.

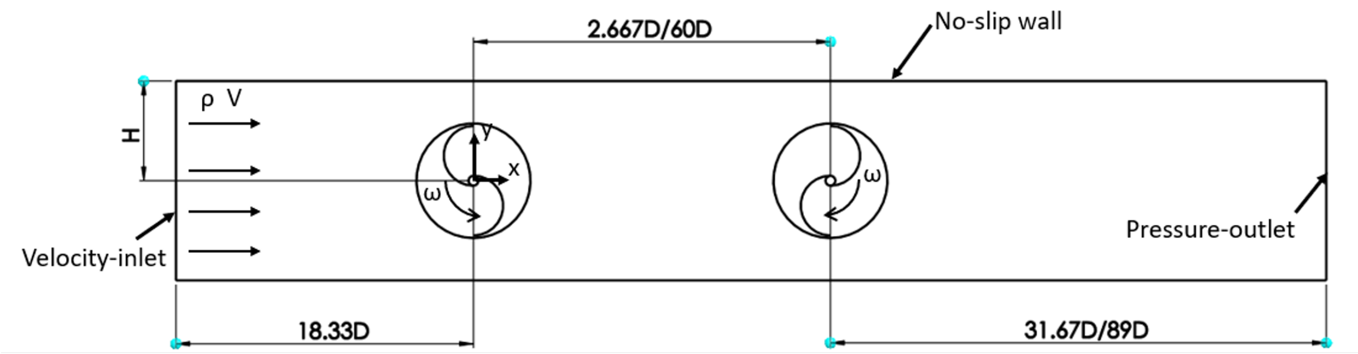

Figure 2. Computational domain and boundary conditions of this study.

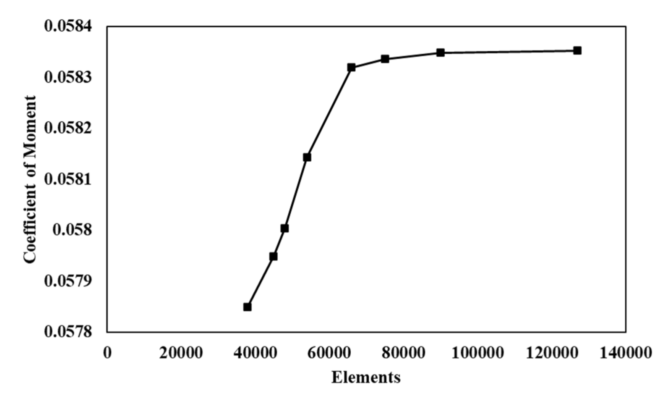

Figure 3. Grid sensitivity used in this study.

$$\frac{\partial u}{\partial x} + \frac{\partial v}{\partial y} = 0 \tag{1}$$

$$\rho\left(\frac{\partial u}{\partial x} + u\frac{\partial u}{\partial x} + v\frac{\partial u}{\partial y}\right) = \rho g_x - \frac{\partial p}{\partial x} + \mu\left(\frac{\partial^2 u}{\partial x^2} + \frac{\partial^2 u}{\partial y^2}\right)$$
$$\rho\left(\frac{\partial v}{\partial x} + u\frac{\partial v}{\partial x} + v\frac{\partial v}{\partial y}\right) = \rho g_y - \frac{\partial p}{\partial y} + \mu\left(\frac{\partial^2 v}{\partial x^2} + \frac{\partial^2 v}{\partial y^2}\right) \tag{2}$$

Where ρ is the fluid density, u and v are the velocity components, x and y are the Cartesian coordinates, p is the pressure, g_x and g_y are the gravitational vectors, and μ is the dynamic viscosity.

2.2. Geometry Model

A 2-dimensional approach was applied in order to investigate the self-starting capability of a twin-hydrokinetic Savonius turbine. A 2-dimensional Savonius turbine geometry used in this study is depicted in Figure 1, with 115 mm endplate diameter (D_o), 60 mm blade diameter (D), and 10 mm shaft diameter (b). The characteristic length of the Savonius turbine (L) was measured between the blades' tips at 110 mm. Using this geometry, the static torque coefficient (C_ts) was observed as the quantitative data. It was calculated using Equation 3.

$$C_\mathrm{ts} = \frac{T_\mathrm{s}}{\frac{1}{2}\rho ARU^2} \tag{3}$$

The above equation could be read as follows: C_ts as the static torque coefficient, T_s as the static torque produced by the turbine, ρ as the fluid density, A as the sweep or frontal area, R as the radius of the turbine rotor, and U as the freestream velocity.

2.3. Computational Domain

An additional turbine was installed horizontally at a range defined as distance levels (T). This was defined as a tandem arrangement. There were two distance levels (T), $2.667D$ and $60D$. The rotational move of the upstream turbine was counterclockwise (CCW), while the downstream turbine was clockwise (CW). The placement of both turbines at $2.667D$ and $60D$ distances is based on the previous research conducted by [22], which concluded that at a distance of $60D$, the upstream turbine no longer influences the downstream turbine. Thus, in this study, the distance between both turbines is varied at $2.667D$ and $60D$ to investigate the impact on the self-starting capability. The twin-hydrokinetic Savonius turbine was applied in a confined channel with six levels of channel width, corresponding to the blockage ratio (ε). The blockage ratio is a nondimensional parameter related to channel width ($2H$) and the turbine's characteristic length (L), where H values are 90, 121, 183, 250, 550, and 1100 mm. In order to obtain the blockage value, the following formula (4) is used.

$$\varepsilon = \frac{L}{2H} \tag{4}$$

From the above equation, ε was the blockage ratio, L was the characteristic length of the Savonius turbine, and H was the distance between the wall and the center of the turbine. The blockage ratio values used in this study were 0.61, 0.45, 0.3, 0.22, 0.1, and 0.05. The inlet side of the computational domain was defined as a velocity inlet at 0.3 m/s, corresponding to the 37000 Reynolds number, and located $10L$ or $18.33D$ from the upstream turbine. The pressure outlet was set at $17.27L$ ($31.67D$) and $48.54L$ ($89D$), referring to both turbines' distances.

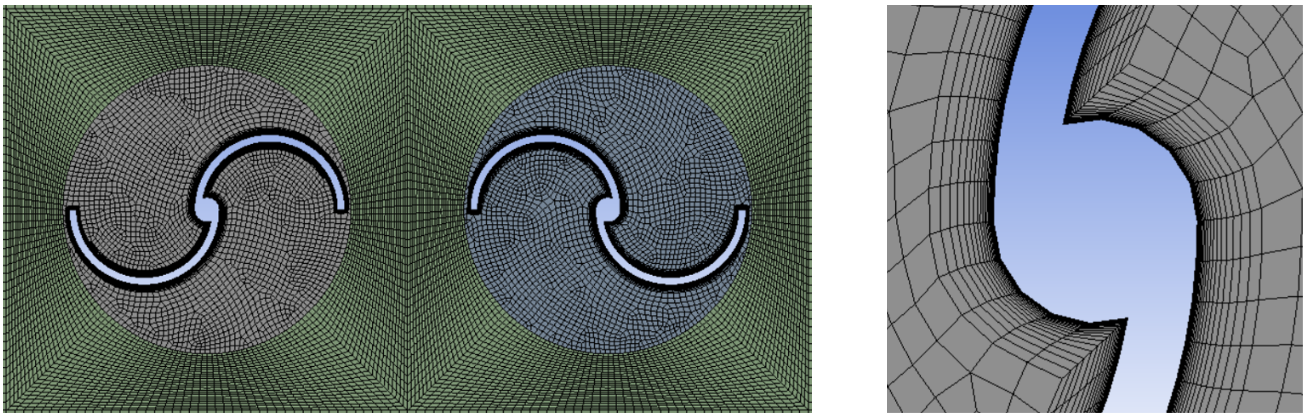

Figure 4. Generated mesh at (a) rotating domain, (b) turbine wall.

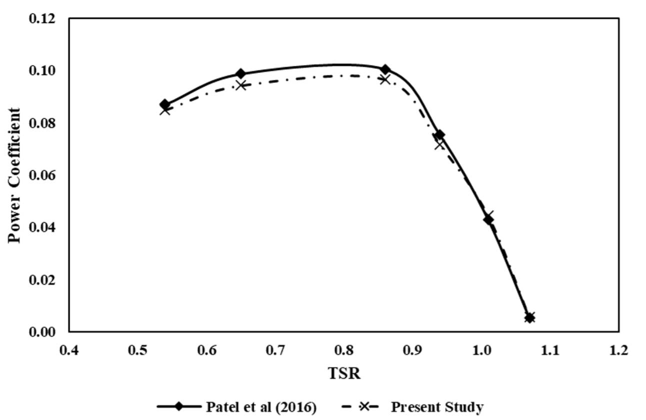

Figure 5. Validation of present numerical study with experiment from [39].

The wall of the channel was in a no-slip condition, in contrast to that of the turbines. Details of the computational domain used in this numerical study are visualized in Figure 2. However, this two-dimensional approach takes place on the midspan of the Savonius turbine; thus, the investigation is limited to the midspan and does not discuss 3D effects such as the aspect ratio of the turbine.

2.4. Grid Sensitivity

The computational domain applied in the present study was discretized after the boundary conditions were defined. The objective of discretization, or meshing, was to partition the computational domain into a number of elements containing nodes in order to solve the continuity and Navier–Stokes equations using a numerical approach. Several mesh levels were generated to obtain an optimum number of elements that no longer produce a high relative error in the results while maintaining computational efficiency. From Figure 3, it is apparent that the optimum number of elements obtained was 66,000 due to the negligible change in the coefficient of moment. Figure 4 illustrates the generated mesh in the rotating domain (Figure 4(a)) and around the turbines (Figure 4(b)). An inflation layer was used to capture the boundary layer development near the turbine wall, with a first-layer thickness of 10^{-4} mm and a total of 20 layers.

2.5. Numerical Setup

Furthermore, a numerical study requires an appropriate setup to solve the governing equations. In the present study, the Reynolds-Averaged Navier–Stokes (RANS) equations were solved using the Realizable k-ε turbulence model with Enhanced Wall Treatment, in accordance with [38]. Steady-state was applied with the purpose of capturing the phenomenon at a certain point in time and velocity. The Coupled scheme was selected for pressure–velocity coupling due to its faster convergence compared to the SIMPLE scheme. Second-order discretization was applied for pressure, velocity, turbulence kinetic energy, and the dissipation rate. The convergence criteria were set to 10^{-5} for all governing equation residuals. The Savonius turbine is rotated with a $10°$ increment angle from $0°$ to $180°$, in order to calculate the static torque coefficient at every azimuth angle (θ).

3. Results and Discussion

3.1. Validation of Numerical Setup

This numerical study was validated using the experimental results reported in [39]. The objective of the validation process is to assess whether the numerical model can accurately predict and represent the physical phenomenon. Figure 5 demonstrates a close agreement in the power coefficient, with an average error of 3.65% between the experimental and numerical results. Therefore, the numerical model developed in this study can be considered valid and reliable for representing the experimental results reported in [39].

3.2. Static Torque Coefficient of T/D 2.667 Turbines

The self-starting capability of the turbine is directly indicated by the static torque coefficient (C_{ts}); positive-

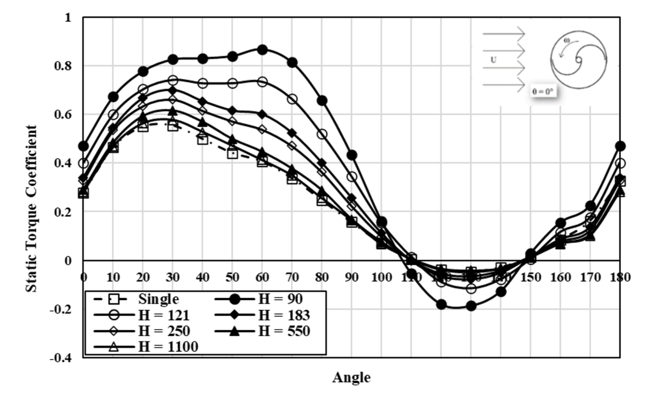

Figure 6. Static Torque Coefficient of T/D 2.667 upstream Savonius turbines at every wall distance (H).

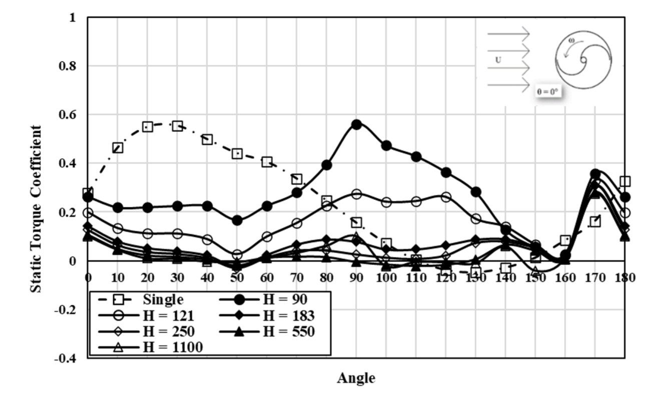

Figure 7. Static Torque Coefficient of T/D 2.667 downstream Savonius turbines at every wall distance.

C_{ts} values across a wide range of azimuth angles (θ) signify a strong ability to start rotating from a standstill, while negative values indicate a 'dead band' where external force is needed. The static torque coefficient (C_{ts}) is linearly correlated with the azimuth angle (θ) of the Savonius turbine. The installation of both turbines in a channel and at a relatively close distance or T/D 2.667 and in a channel has influenced the upstream turbine's static torque coefficient. The upstream turbine's C_{ts} curve compared to the conventional turbine is depicted in Figure 6. Due to its position, the upstream turbine produces a similar C_{ts} curve to the conventional turbine with an increase, as a consequence of the wall channel's presence. An increase in channel width leads to the enhancement of C_{ts} and subsequently shifts the optimum θ. Optimum C_{ts} is obtained at H 90 mm, with positive C_{ts} occurring at $\theta = 0°$-$100°$ and $150°$-$180°$, while $60°$ is the optimum θ with 113.75% improvement of C_{ts} compared with the single turbine from 0.4059 to 0.8676. This phenomenon indicates that the upstream turbine is experiencing an improvement in self-starting capability, with the majority of C_{ts} positive values as evidence, and only a few angles with C_{ts} negative values. $\theta = 60°$ is the optimum angle with higher C_{ts} compared with others due to the position of the advancing blade. The inner side of the related blade begins to align with the flow direction and is associated with the higher momentum taken by the blade rather than other θ. The upstream Savonius turbine also experiences an improvement in C_{ts} at H 121-1100 mm at $\theta = 60°$ with C_{ts} values of 0.734, 0.5996, 0.5372, 0.4458, and 0.4114; this enhancement corresponds with 80.83%, 47.72%, 32.35%, 9.83%, and 1.36% compared with the single turbine.

The increase in channel width reduces the upstream turbine's C_{ts}, following the shifting of the optimum θ to $30°$. This phenomenon can be attributed to the reduction in momentum directed toward the upstream turbine as the channel width increases, which is visualized in Figure 6. At H 1100 mm, the C_{ts} curve of the upstream turbine resembles the conventional turbine due to suppressed wall influence on the momentum towards the upstream turbine. This is evidenced by quite similar C_{ts} values at 0.576 and 0.5535 at H 1100 mm and the conventional turbine at an optimum θ of $30°$. A positive C_{ts} of the T/D 2.667 upstream turbine in all blockage ratios spotted at similar angles, $\theta = 0°$-$100°$ and $150°$-$180°$, while for the negative values were at $\theta = 110°$-$140°$ for the negative values. This means that at a related angle of positive C_{ts} value, the upstream turbine's self-starting capability is better. On the other side, when the turbine is at $\theta = 110°$-$140°$, producing a negative value of C_{ts}, its self-starting capability is reduced. Hence, the upstream turbine in a lower confined channel requires an additional effort in order to rotate independently.

The proximity of the upstream and downstream turbines, since $T/D = 2.667$, accounts for the upstream turbine to influence the downstream turbine massively. As shown in Figure 7, the downstream turbine's C_{ts} curve significantly differs from the conventional or single turbine. However, with the higher confined level, the downstream turbines continue to experience an increase in C_{ts}. The channel influenced the phenomenon by suppressing wake-shedding from the upstream turbine towards the T/D 2.667 downstream turbine. Thus, the H 90 and 121 mm downstream turbines exhibit a positive value of C_{ts} in almost all θ. An increase in C_{ts} is evident in the H 90 mm downstream turbine, particularly in $\theta = 80°$-$150°$, which corresponds to a better self-starting capability of the downstream turbine. When $\theta < 80°$, the downstream turbine experiences lower C_{ts} values and self-starting capability, compared to the single turbine.

On the other hand, the H 121 mm downstream turbine experiences a better self-starting capability in $\theta = 90°$-$150°$. In contrast, a lower self-starting capability occurs in $\theta < 90°$. An optimum C_{ts} value based on Figure 7 is at $\theta = 90°$ and H 90 mm. This condition is influenced by the position of the advancing blade in the related angle. Since the advancing blade aligns with the flow direction, it collects the reattachment shear layer from the upstream separation and directs the momentum to focus on the inner side of the downstream turbine's advancing blade, which possesses a higher drag coefficient

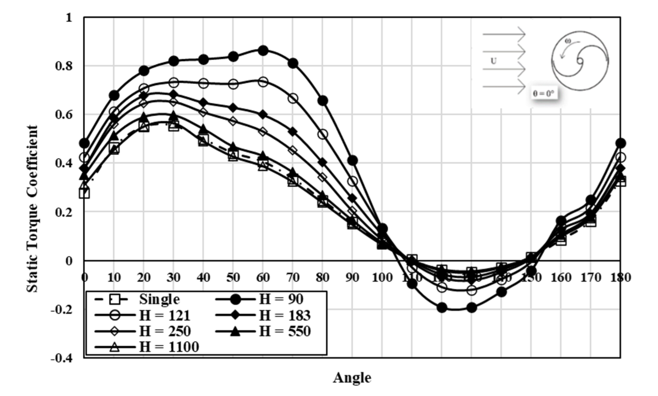

Figure 8. Static Torque Coefficient of T/D 60 upstream Savonius turbines at every wall distance.

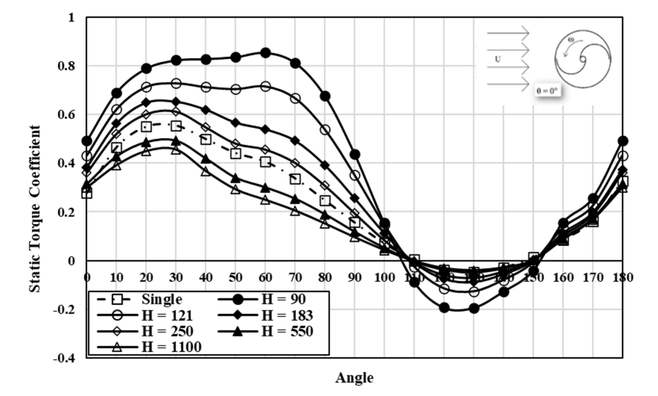

Figure 9. Static Torque Coefficient of T/D 60 downstream Savonius turbines at every wall distance.

due to the blade geometry. That is the main factor that influences the higher C_{ts} of H 90 and 121 mm downstream turbines in $\theta = 90°$. Generally, the optimum θ for the downstream turbine occurs at $\theta = 90°$ for H 90 and 121 mm, with C_{ts} values of 0.5612 and 0.2748, corresponding to the 229.21% and 75.26% improvement compared with the single turbine with a value of 0.1568, respectively.

As the confined level decreases, the suppressed wake becomes wider and covers the T/D 2.667 downstream turbine. The related phenomenon is proven by the reduction of the downstream turbine's C_{ts}, which also corresponds to the similarity of self-starting capability at H183-1100 mm. The phenomenon is influenced by lower momentum towards the downstream turbine, since the turbine is covered by the upstream turbine's wake-shedding. At a limited angle, $\theta = 120°$-$140°$, the downstream turbine is able to generate a better C_{ts}, which indicates a better self-starting of the downstream turbine compared to the single turbine. A single turbine generates a C_{ts} value of -0.0466 at $\theta = 130°$, and a noticeable increase occurs at a similar θ for entire configurations, with C_{ts} values of -0.0102, 0.0062, 0.0724, 0.0866, 0.1723, and 0.2825 for H 1100, 550, 250, 183, 121, and 90 mm, respectively. The increase corresponds to 78.11%, 113.31%, 255.37%, 285.84%, 469.74%, and 706.22% improvement, respectively.

3.3. Static Torque Coefficient of T/D 60 Turbines

According to [22], since the wake-shedding of the upstream turbines no longer influences the downstream turbines, the required horizontal distance (T) for counter-rotating twin-hydrokinetic Savonius turbines is $60D$. It leads to the similarity of static torque coefficients of the upstream and downstream turbines; however, the presence of the channel effect contributes to the extremely increasing static torque coefficient of both turbines. As demonstrated in Figures 8 and 9, the upstream and downstream turbines share a similarity of C_{ts} at H 90-1100 mm, respectively.

The upstream and downstream turbines with H 90 mm experience a significant increase in C_{ts} compared to the single turbine at $\theta = 60°$, from 0.4059 to 0.8649, corresponding to a 113.08% improvement. At this angle, the advancing blade is approaching the maximum drag circumstance due to its alignment with the flow direction; hence, the acceptance of momentum on the inner side of the blade turns greater when compared to other angles. During H 121 mm, the optimum C_{ts} also occurs at $\theta = 60°$ with 81.08% enhancement from 0.4059 to 0.735. Reducing the confinement level causes a noticeable C_{ts} reduction in both H183-1100 turbines, and transferring the angles with optimum C_{ts} to $\theta = 30°$. Although the reduction, the C_{ts} values of H 183, 250, and 550 mm experience an increase at $\theta = 30°$, from 0.5535 to 0.682, 0.651, and 0.5968, corresponding to 23.22%, 17.62%, and 7.82% improvement, respectively. At H 1100 mm, the upstream turbine's C_{ts} curve matches the single turbine, indicating that the channel effect at this confined level has vanished. H 90-1100 mm turbines produce a uniformity curve of C_{ts} positive values in $\theta = 0°$-$100°$ and $160°$-$180°$, respectively. This emphasizes that H 90-1100 mm upstream and downstream turbines generate a better self-starting capability at related angles. On the other hand, negative C_{ts} values are generated at $\theta = 110°$-$150°$ in all confinement levels, which implies an inferior self-starting capability of both turbines.

As the distance increases, the upstream becomes less influential on the downstream turbine's self-starting capability. Figure 9 exhibits similar curves of downstream turbines' C_{ts} compared to the upstream and the single turbine, as proven by the similarity of positive static torque values at the identical angles, in $\theta = 0°$-$100°$ and $160°$-$180°$. The optimum θ for H 90 mm is obtained at $\theta = 60°$, with a 110.22% improvement, from 0.4059 to 0.8533. Furthermore, for H 121-1100 mm, the optimum θ is achieved at a similar angle with the single turbine, at $\theta = 30°$. The enhancement compared to the single turbine happens at H 121, 183, and 250 mm, with 31.53%, 17.8%, and 10.49% improvement, respectively. Static torque coefficient in H 550 and 1100 mm shows a visibly lower value than the single turbine, with values of 0.492 and 0.455, or a 11.1% and 17.8% decrease, respectively. Hypothetically,

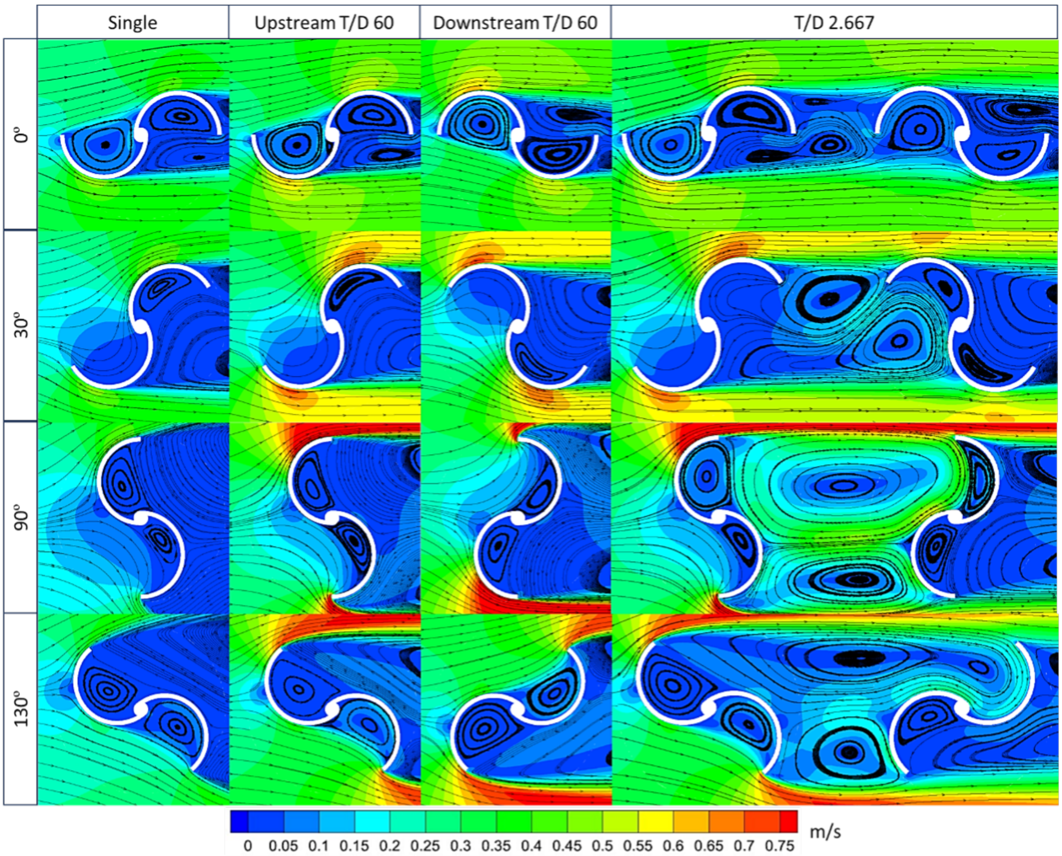

Figure 10. Velocity contour of Savonius turbines at H 90 mm and θ of $0°$, $30°$, $90°$, and $130°$.

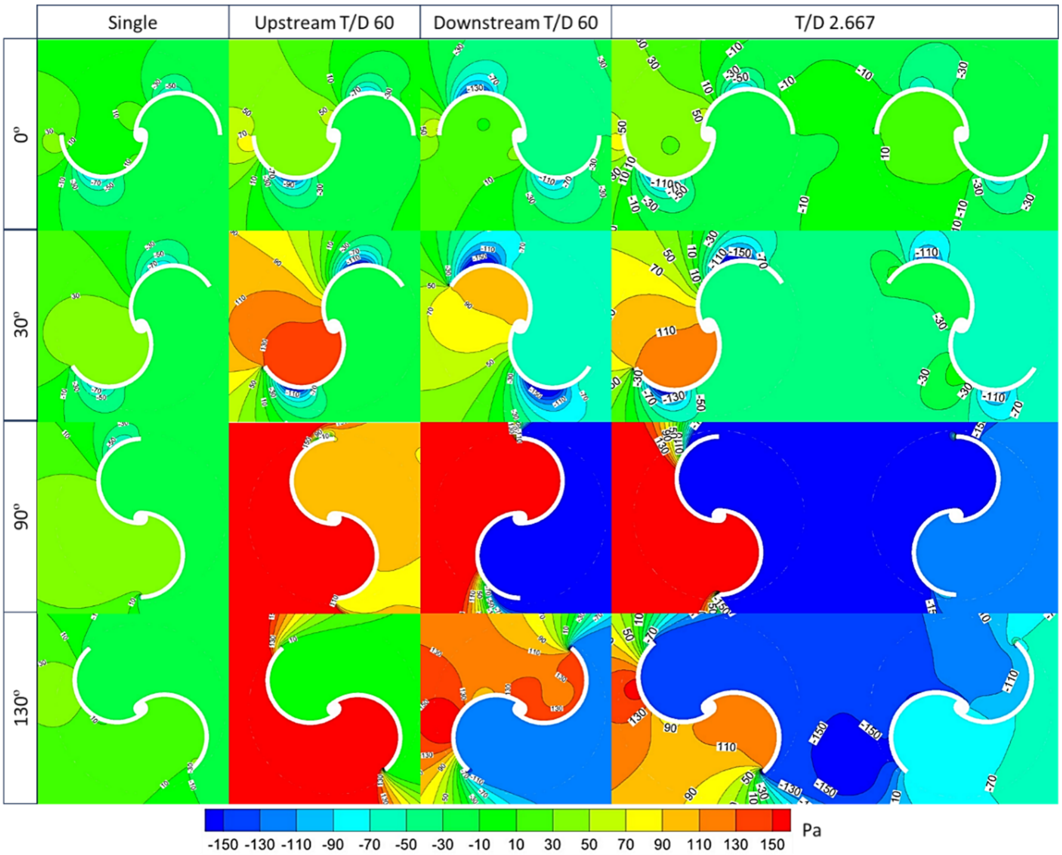

Figure 11. Pressure distribution at H 90 mm and θ of $0°$, $30°$, $90°$, and $130°$.

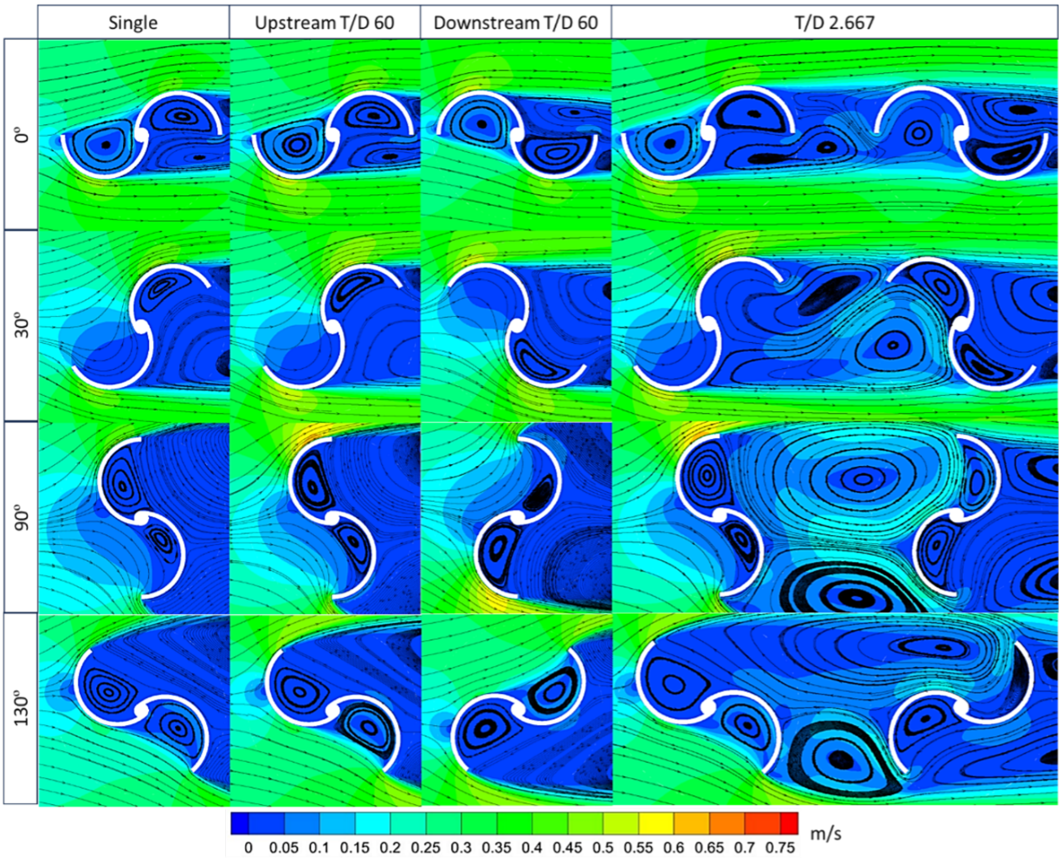

Figure 12. Velocity contour of Savonius turbines at H 183 mm and θ of $0°$, $30°$, $90°$, and $130°$.

this decrease is due to the greater and more extensive wake-shedding from the upstream turbine, which has not fully relaxed; consequently, the momentum towards the downstream turbine has reduced compared to the upstream and single Savonius turbine. Therefore, a corresponding self-starting capability of the downstream turbine also increases in the range of positive C_{ts} angles, $\theta = 0°$-$100°$ and $160°$-$180°$. Throughout $\theta = 110°$-$150°$, negative C_{ts} values were generated.

3.4. Flow Visualization and Pressure Distribution

Figure 10-11 shows velocity and pressure contours of the Savonius turbines at H 90 mm compared to the conventional turbine at $\theta = 0°$, $30°$, $90°$, and $130°$. From the velocity contour, it is known that there is an enhancement at the convex side of the advancing and returning blades at T/D 60. This enhancement generates a nozzle effect due to the proximity of the wall to the turbines and influences the wake intensity of the upstream turbine as visualized at $\theta = 90°$ and $130°$. The similarity in velocity contour evidence that the upstream wake diminishes; hence, the downstream turbine is able to generate similar C_{ts} to the upstream. The wall channel effect suppresses the wake of the upstream turbine at $\theta = 90°$; hence, the downstream turbine is able to produce a similar C_{ts}. At the closest distance, T/D 2.667, the wake intensity of the upstream significantly influences the downstream turbine. However, at $\theta = 90°$, it can be observed that due to the wall effect, the wake of the upstream turbine is suppressed. Furthermore, the downstream turbine displays a quite similar flow pattern near the turbine wall. This influences the self-starting capability of the downstream turbine, as visualized in Figure 11. Torque produced by the Savonius turbine is generated due to the pressure drop at the advancing blade, which is evidence of the greater C_{ts} produced by the upstream and downstream turbines at T/D 60 compared to the conventional. A greater pressure drop is experienced at $\theta = 30°$ and $130°$ due to the higher pressure at the concave side than the convex side, and the related pressure drop is also greater than conventional at similar angles. On the other hand, at $\theta = 90°$, the upstream turbine no longer experiences a great pressure drop due to being covered by a high-pressure area on the convex and concave sides. Moreover, a massive pressure drop occurs at the downstream turbine as shown in Figure 11. This phenomenon leads to the C_{ts} improvement of the downstream turbine, which has the highest C_{ts} at $\theta = 90°$ among other configurations (H) and a single turbine.

Conversely, the proximity of the upstream and downstream turbines or T/D 2.667 generates a decline in C_{ts} produced by the downstream. As shown in Figure 11, the downstream turbine at T/D 2.667 is covered by a low-pressure area, which influences the pressure drop experienced by the downstream. The reduction in pressu-

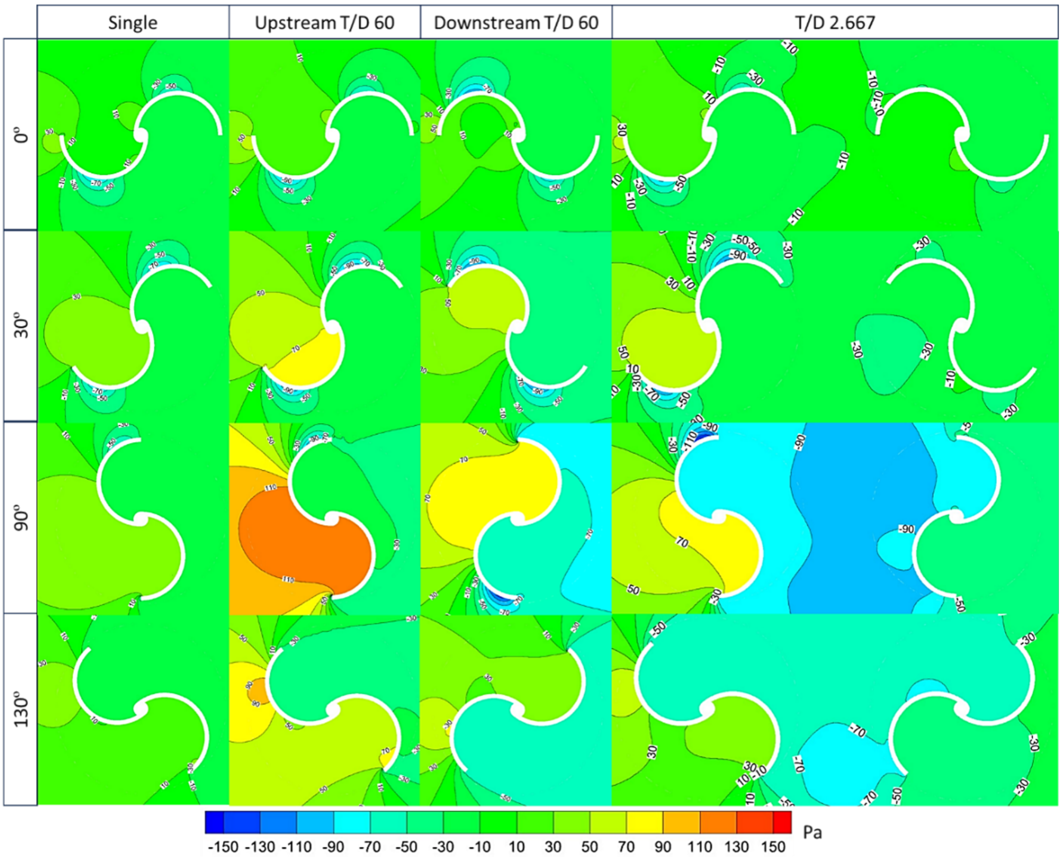

Figure 13. Pressure distribution of Savonius turbines at H 183 mm and θ of $0°$, $30°$, $90°$, and $130°$.

re drop, particularly at $\theta = 0°$ and $30°$, leads to the lower production of C_{ts} by the downstream. However, at $\theta = 90°$ and $130°$, as a result of the closest distance of the turbines, the upstream provides an external force toward the downstream. This external force experienced by the downstream increases the self-starting capability, which is greater than that of the upstream and conventional turbine. In addition, due to the higher static torque generated by the Savonius turbines installed in a water channel, it is possible for the Savonius hydrokinetic turbines to produce a greater dynamic torque once the turbine is in motion. This is justified by the pressure distribution in Figure 11. Figure 11 captures the pressure distribution of the Savonius turbine in a water channel with H 90 mm. It is known that the turbines experienced a massive pressure drag, which leads to the greater pressure drop of the concave and convex sides of the turbine. While the turbine is in motion, this greater pressure drop enhances the dynamic torque produced by the turbine and improves its efficiency. The operational range (TSR) is also wider due to higher kinetic energy and greater pressure drop experienced by the turbine.

Moreover, Figures 12-15 show the flow visualization and pressure distribution of Savonius turbines at H 183 mm and H 1100 mm, respectively. An increase in wall distance reduces its influence on the turbine at H 183 mm, as shown in Figure 12. A nozzle effect occurs at the convex side of the upstream and downstream at T/D 60, with a noticeable effect that can be seen at $\theta = 90°$. During H 90 mm, the wake is suppressed by the presence of the channel wall, which gradually widens due to the increase in the wall distance (H). This is justified by a relatively similar flow pattern experienced by the upstream and downstream turbines at T/D 60 for $\theta = 0°$, $30°$, $90°$, and $130°$. At T/D 2.667, the greater upstream wake intensity strongly affects the self-starting capability of the downstream turbine. It can be assumed that the increase in the wall distance (H) is followed by a decline in the self-starting capability of the downstream turbine at T/D 2.667. A reduction in pressure drop experienced by the downstream turbine plays an important role in the self-starting capability. As shown in Figure 13, the downstream turbine is covered by a negative pressure area, which significantly influences the reduction of the C_{ts} curve of the downstream turbine. Pressure drop reduction also occurs at the upstream turbine due to the decrease in the wall effect toward the turbine. Furthermore, the upstream turbine at T/D 2.667 experiences the pressure drop of the convex and concave sides of the advancing blade and provides a greater C_{ts} compared to the conventional. At the large distance, T/D 60, the upstream and downstream show a similar C_{ts} curve to the conventional. Figure 13 depicts the increased pressure drop that occurs at $\theta = 0°$, $30°$, $90°$, and $130°$ at T/D 60, which enhances the C_{ts} value of both turbines rather than the conventional turbine.

According to [19], when the blockage ratio level (ε)

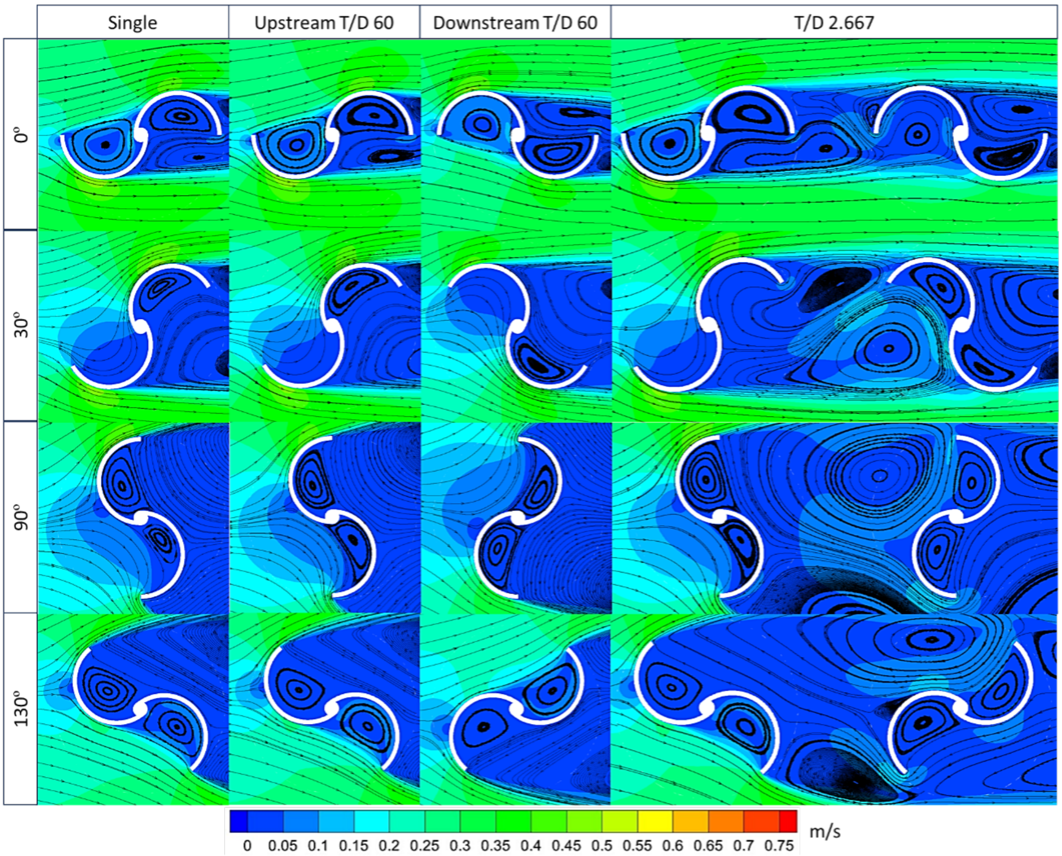

Figure 14. Velocity contour at H 1100 mm and θ of 0°, 30°, 90°, and 130°.

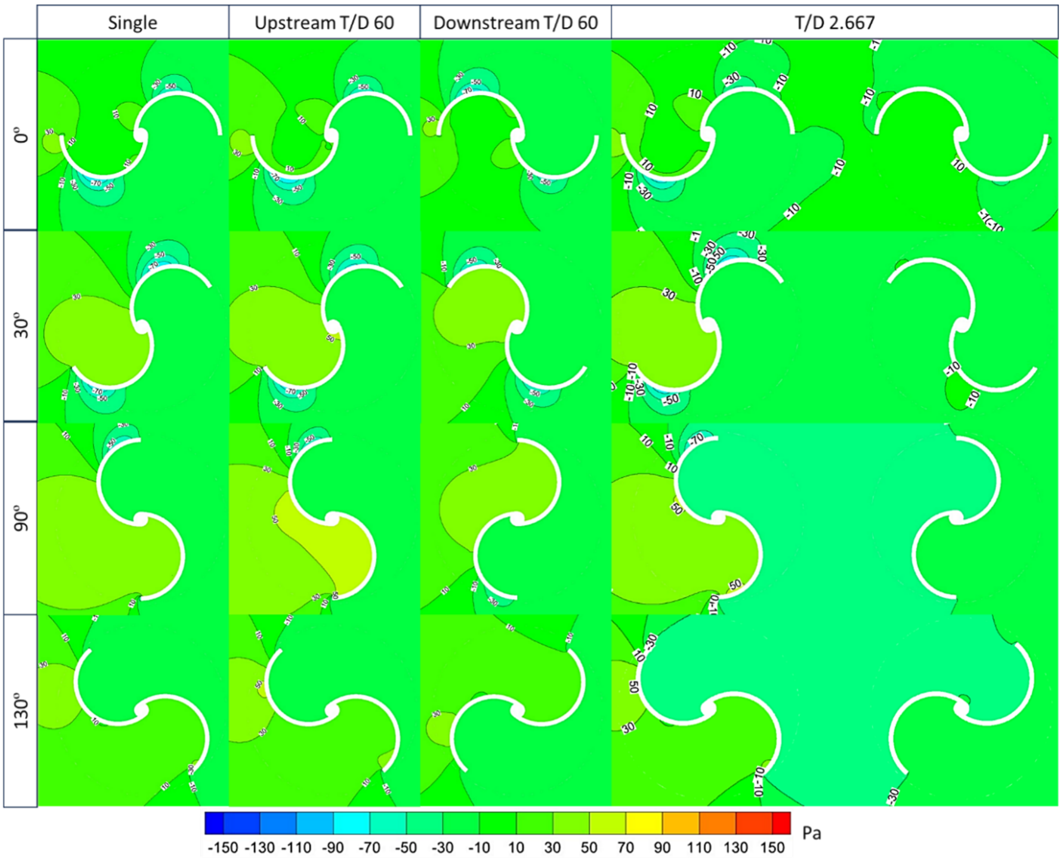

Figure 15. Pressure distribution at H 1100 mm and θ of 0°, 30°, 90°, and 130°.

is lower than 30%, the Savonius turbines no longer require a correction. At H 1100 mm, the blockage effect on the Savonius turbines diminishes; hence, the C_{ts} of the upstream T/D 2.667 and 60 are quite similar to the conventional, as well as the flow pattern around the upstream and downstream T/D 60, as shown in Figure 14. It indicates that the self-starting capability of both turbines is no longer affected by the wall channel. However, due to the strong influence of the upstream wake at the closest distance, T/D 2.667, the downstream is in the negative pressure area. This occurs as a consequence of the large wall distance, which no longer suppresses the wake of the upstream. Figure 15 clearly provides proof of the C_{ts} reduction at H 1100 mm as part of the larger wall channel distance. The upstream T/D 2.667 and 60 share a similar pressure drop to the conventional turbine, and become evidence of the similar C_{ts} curve. A wider area of the upstream wake, as discussed before, deteriorates the self-starting capability of T/D 2.667 and 60 downstream turbines. At T/D 2.667, the downstream turbine dominantly generates a lower C_{ts} value due to the locations with low pressure. Moreover, in this area, the downstream turbine is not able to produce a positive torque due to the poor pressure drop. On the other hand, due to the large distance at T/D 60, the downstream turbine is able to generate a positive torque, similar to the upstream and conventional. Yet, the downstream turbine obtained a lower curve than the upstream and conventional due to the intense wake from the upstream turbine. An interaction between upstream and downstream occurs as a result of a larger wake, which requires further distance to minimize the influence on the downstream turbine.

4. Conclusions

The vicinity of the upstream and downstream turbines, as well as the channel effects, are the primary factors influencing the static torque coefficient related to the self-starting capability. At $T/D = 2.667$, the upstream turbine's static torque coefficient increases compared to that of a single turbine, particularly at $H = 90$ mm and $\theta = 60°$, with 113.75% from 0.4059 to 0.8676. However, due to the proximity of the two turbines and the channel effects, the optimum static torque coefficient of the downstream turbine, which is associated with improved self-starting capability, occurs at $H = 90$ mm and $H = 121$ mm and $\theta = 90°$. This enhancement corresponds to 229.21% and 75.26% improvement compared with the single turbine, from values of C_{ts} 0.1568 to 0.5612 and 0.2748, respectively. For $T/D = 60$, the static torque coefficients of both turbines show similar values due to the larger spacing distance. The optimum θ for the upstream turbines occurred at $\theta = 60°$ for H 90 and 121 mm with 113.08% and 81.08% improvement, compared to the single turbine from 0.4059 to 0.8649 and 0.735, respectively. Furthermore, for the downstream turbine, the optimum θ at $60°$ only occurs at H 90 mm with 110.22% improvement from 0.4059 to 0.8533. Reducing the confined level, the optimum θ shifts to $30°$ for the upstream turbine at H 183-550 mm, with 23.22%, 17.62%, and 7.82% enhancement. In addition, the optimum C_{ts} for the downstream turbine is obtained at a similar angle, $\theta = 30°$, with 31.53%, 17.8%, and 10.49% improvement for H 121, 183, and 250 mm, respectively. On the other hand, since the wall effect decreases, the downstream turbines at H 550 and 1100 mm produce a lower C_{ts} value with 11.1% and 17.8% decreases, respectively. This condition causes the self-starting capability of both turbines to become similar and slightly improved compared to that of a single turbine. From this study, it can be concluded that the installation of Savonius hydrokinetic turbines in a water channel influences the static torque of the turbine, which enhances the self-starting capability. In practice, the installation in a water channel allows the turbine to generate a higher dynamic torque and greater power harvesting. For future work, it is recommended to investigate a wider range of velocities to observe the interaction between the Reynolds number and blockage effects. In addition, further study is needed to determine the precise distance between $T/D = 2.667$ and 60 at which the interference of the upstream wake on the downstream turbine becomes negligible, and to conduct a three-dimensional study for further and comprehensive investigation.

Acknowledgments

The authors would like to express gratitude to the Mechanical Engineering Department of Institut Teknologi Sepuluh Nopember for granting permission to utilize the Computational Laboratory. All authors have declared that there is no conflict of interest.

References

[1] M. J. Khan, M. T. Iqbal, and J. E. Quaicoe, "A technology review and simulation based performance analysis of river current turbine systems," in *2006 Canadian Conference on Electrical and Computer Engineering*, pp. 2288–2293, 2006.

[2] A. Kumar and R. P. Saini, "Performance parameters of savonius type hydrokinetic turbine – a review," *Renewable and Sustainable Energy Reviews*, vol. 64, pp. 289–310, 2016.

[3] P. A. Setiawan, T. Yuwono, and W. A. Widodo, "Numerical simulation on improvement of a savonius vertical axis water turbine performance to advancing blade side with a circular cylinder diameter variations," *IOP Conference Series: Earth and Environmental Science*, vol. 200, no. 1, p. 012029, 2018.

[4] P. A. Setiawan, T. Yuwono, and W. A. Widodo, "Effect of a circular cylinder in front of advancing blade on the savonius water turbine by using transient simulation," *International Journal of Mechanical and Mechatronics Engineering*, vol. 19, no. 1, pp. 151–159, 2019.

[5] P. A. Setiawan, T. Yuwono, and W. A. Widodo, "Numerical study of the stagger angle effect of a circular cylinder installed in front of returning blade toward the vertical axis savonius water turbine performance," *Journal of Physics: Conference Series*, vol. 1179, no. 1, p. 012107, 2019.

[6] P. A. Setiawan, A. W. Husodo, F. Hamzah, T. Yuwono, and W. A. Widodo, "Performance analysis of savonius turbine disturbed by cylinder in front of returning with variation of distance to perpendicular fluid flow," *International Journal of Mechanical Engineering and Robotics Research*, vol. 11, no. 10, pp. 761–766, 2022.

[7] D. F. Shabrina and T. Y. Yuwono, "Performance of a savonius turbine with circular cylinders installed in front of the convex blade and next to the concave blade," *The International Journal of Mechanical Engineering and Sciences*, vol. 9, no. 1, pp. 1–8, 2025.

[8] T. Y. Yuwono, B. R. Ananto, S. Paramesti, F. M. Mahardina, E. Lisdarina, V. N. Arif, D. Jeremia, M. L. Budihartono, and A. Shuhufam, "Enhancing savonius turbine self-starting capability by installing a circular cylinder in front of returning turbine blade," *The International Journal of Mechanical Engineering and Sciences*, vol. 5, no. 1, pp. 16–23, 2021.

[9] T. Yuwono, A. Latip, N. P. Putri, M. Ubaidillah, E. N. Mazhilna, C. Ariyanto, U. Andaryani, A. Fauzi, W. A. Widodo, and B. A. Dwiyantoro, "The effect of width of single curtain on the performance of savonius wind turbine," in *AIP Conference Proceedings*, vol. 1983, p. 020023, 2018.

[10] M. Mosbahi, A. Ayadi, Y. Chouaibi, Z. Driss, and T. Tucciarelli, "Performance study of a helical savonius hydrokinetic turbine with a new deflector system design," *Energy Conversion and Management*, vol. 194, pp. 55–74, 2019.

[11] N. P. Putri, T. Yuwono, J. Rustam, P. Purwanto, and G. Bangga, "Experimental studies on the effect of obstacle upstream of a savonius wind turbine," *SN Applied Sciences*, vol. 1, no. 1216, pp. 1–7, 2019.

[12] M. B. Salleh, N. M. Kamaruddin, and Z. Mohamed-Kassim, "The effects of deflector longitudinal position and height on the power performance of a conventional savonius turbine," *Energy Conversion and Management*, vol. 226, p. 113584, 2020.

[13] B. D. Altan and A. Gungor, "Examination of the effect of triangular plate on the performances of reverse rotating dual savonius wind turbines," *Processes*, vol. 10, no. 11, p. 2278, 2022.

[14] H. Aboujaoude, F. Beaumont, S. Murer, G. Polidori, and F. Bogard, "Aerodynamic performance enhancement of a savonius wind turbine using an axisymmetric deflector," *Journal of Wind Engineering and Industrial Aerodynamics*, vol. 220, p. 104882, 2022.

[15] A. Hesami, A. H. Nikseresht, and M. H. Mohamed, "Feasibility study of twin-rotor savonius wind turbine incorporated with a wind-lens," *Ocean Engineering*, vol. 247, p. 110654, 2022.

[16] M. B. Salleh, N. M. Kamaruddin, and Z. Mohamed-Kassim, "Experimental investigation on the effects of deflector angles on the power performance of a savonius turbine for hydrokinetic applications in small rivers," *Energy*, vol. 247, p. 123432, 2022.

[17] Y. Chen, Y. Chen, J. Zhou, P. Guo, and J. Li, "Optimization and performance study of bidirectional savonius tidal turbine cluster with deflectors," *Energy Conversion and Management*, vol. 283, p. 116947, 2023.

[18] M. Nakajima, S. Iio, and T. Ikeda, "Performance of savonius rotor for environmentally friendly hydraulic turbine," *Journal of Fluid Science and Technology*, vol. 3, no. 3, pp. 420–429, 2008.

[19] K. Golecha, T. I. Eldho, and S. V. Prabhu, "Study on the interaction between two hydrokinetic savonius turbines," *International Journal of Rotating Machinery*, vol. 2012, p. 581658, 2012.

[20] Y. Zhang, C. Kang, H. Zhao, and S. Teng, "Effects of in-line configuration of drag-type hydrokinetic rotors on inter-rotor flow pattern and rotor performance," *Energy Conversion and Management*, vol. 196, pp. 44–55, 2019.

[21] A. K. Nag and S. Sarkar, "Performance analysis of helical savonius hydrokinetic turbines arranged in array," *Ocean Engineering*, vol. 241, p. 110020, 2021.

[22] R. Effendi, "Studi numerik dua turbin air savonius tersusun tandem dan berputar berlawanan arah," master's thesis, Institut Teknologi Sepuluh Nopember, 2023.

[23] Y. E. Priandika, T. Y. Yuwono, and R. Hermawan, "Numerical study of tandem installation of twin savonius hydrokinetic turbines on pltu paiton cooling water channel," in *E3S Web of Conferences*, vol. 517, p. 10001, 2024.

[24] Y. Chen, D. Zhang, P. Guo, Q. Hu, and J. Li, "A comparative analysis of 2-d and 3-d simulation for savonius hydrokinetic turbine array," *Ocean Engineering*, vol. 295, p. 116909, 2024.

[25] A. F. Aulina and H. Hasbiyati, "Aerodynamic performance analysis of tandem savonius wind turbines influenced by lateral gap from adjacent wall," *The International Journal of Mechanical Engineering and Sciences*, vol. 10, no. 1, pp. 1–10, 2026.

[26] A. N. Izzah, T. Yuwono, D. F. Shabrina, H. F. N. Faurizki, and A. F. Aulina, "Numerical study of the performance of twin savonius hydrokinetic turbines with adjacent advancing blades in a side-by-side configuration placed in a narrow channel," *Renewable Energy*, vol. 264, p. 125601, 2026.

[27] A. H. Elbatran, Y. M. Ahmed, and A. S. Shehata, "Performance study of ducted nozzle savonius water turbine, comparison with conventional savonius turbine," *Energy*, vol. 134, pp. 566–584, 2017.

[28] V. Patel, T. I. Eldho, and S. V. Prabhu, "Velocity and performance correction methodology for hydrokinetic turbines experimented with different geometry of the channel," *Renewable Energy*, vol. 131, pp. 1300–1317, 2019.

[29] H. L. Bai, C. M. Chan, X. M. Zhu, and K. M. Li, "A numerical study on the performance of a savonius-type vertical-axis wind turbine in a confined long channel," *Renewable Energy*, vol. 139, pp. 102–109, 2019.

[30] S. Mauro, S. Brusca, R. Lanzafame, and M. Messina, "Cfd modeling of a ducted savonius wind turbine for the evaluation of the blockage effects on rotor performance," *Renewable Energy*, vol. 141, pp. 28–39, 2019.

[31] A. K. Nag and S. Sarkar, "Experimental and numerical study on the performance and flow pattern of different savonius hydrokinetic turbines with varying duct angle," *Journal of Ocean Engineering and Marine Energy*, vol. 6, pp. 31–53, 2020.

[32] A. Bizhanpour, N. Hasanzadeh, A. F. Najafi, and F. Magagnato, "Investigation of different deflector geometry and mechanism effect on the performance of an in-pipe hydro savonius turbine," *Applied Energy*, vol. 350, p. 121697, 2023.

[33] D. Zhang, P. Guo, Y. Cheng, Q. Hu, and J. Li, "Analysis of blockage correction methods for high-solidity hydrokinetic turbines: Experimental and numerical investigations," *Ocean Engineering*, vol. 283, p. 115185, 2023.

[34] Y. Murai, T. Umemura, H. J. Park, Y. Horimoto, and Y. Tasaka, "Experimental and theoretical fluid dynamics of spherical savonius turbines operated in pipe flows," *Journal of Fluids and Structures*, vol. 127, p. 104105, 2024.

[35] C. M. Niebuhr, M. van Dijk, V. S. Neary, and J. N. Bhagwan, "A review of hydrokinetic turbines and enhancement techniques for canal installations: Technology, applicability and potential," *Renewable and Sustainable Energy Reviews*, vol. 113, p. 109240, 2019.

[36] A. Abutunis and V. G. Menta, "Comprehensive parametric study of blockage effect on the performance of horizontal axis hydrokinetic turbines," *Energies*, vol. 15, no. 7, p. 2585, 2022.

[37] G. Saini and R. P. Saini, "Clearance and blockage effects on hydrodynamic performance of hybrid hydrokinetic turbine," *Sustainable Energy Technologies and Assessments*, vol. 57, p. 103210, 2023.

[38] A. Dewan, S. S. Tomar, A. K. Bishnoi, and T. P. Singh, "Computational fluid dynamics and turbulence modelling in various blades of savonius turbines for wind and hydro energy: Progress and perspectives," *Ocean Engineering*, vol. 283, p. 115168, 2023.

[39] V. Patel, G. Bhat, T. I. Eldho, and S. V. Prabhu, "Influence of overlap ratio and aspect ratio on the performance of savonius hydrokinetic turbine," *International Journal of Energy Research*, vol. 41, no. 6, pp. 829–844, 2017.